I&EC research
Industrial & Engineering Chemistry Research

pubs.acs.org/IECR

Article

Toluene Abatement by Simultaneous Adsorption and Oxidation over Mixed-Metal Oxides

Busuyi O. Adebayo, Anirudh Krishnamurthy, Ali A. Rownaghi, and Fateme Rezaei*

Cite This: https://dx.doi.org/10.1021/acs.iecr.0c02550

Read Online

ACCESS | Metrics & More | Article Recommendations | Supporting Information

ABSTRACT: Development of integrated processes that can concentrate and oxidize volatile organic compounds (VOCs) from process streams or polluted air in an adsorptive reactor provides a cost-effective alternative to current VOC abatement technologies. Here, we report simultaneous adsorption and oxidation of toluene as a VOC model compound over TiO_2/SiO_2 and ZrO_2/SiO_2 mixed-metal oxides (MMOs) with varied compositions. These MMOs were investigated for their equilibrium adsorption capacity and dynamic performance at room temperature (25 °C), as well as their catalytic activity at 250 °C. The adsorption isotherms indicated that equilibrium capacity varies dramatically with TiO_2 and ZrO_2 loading, and the highest toluene uptake was reached over TiO_2/SiO_2 with 8 wt % TiO_2 and ZrO_2/SiO_2 with 13 wt % ZrO_2 (3.9 and 2.9 mmol/g, respectively) at 27 mmHg and 25 °C. Moreover, the integrated capture−oxidation results revealed that Ti-based MMOs are more efficient than Zr-based materials by displaying higher dynamic capacity and toluene conversion as a result of higher surface area and pore volume, surface defects, and hydroxyl groups. The TiO_2/SiO_2 with 8 wt % TiO_2 loading exhibited a dynamic (pseudoequilibrium) adsorption capacity of 3.8 mmol/g and a toluene conversion of 86%. Post oxidative chemical analysis further revealed the retention of materials structure with little coke formation, which highlighted the repeated and sustainable applicability of these materials in VOC abatement processes.

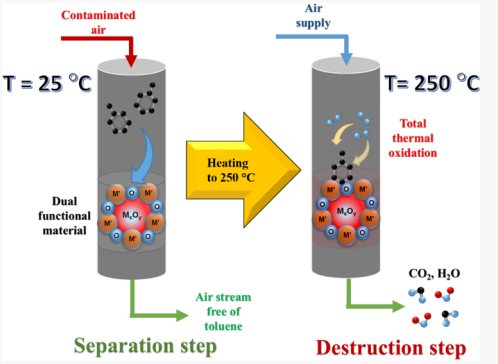

1. INTRODUCTION

Pollution-prevention technologies for abatement of volatile organic compounds (VOCs) usually follow two patterns: removal or destruction. In these processes, the VOC is captured before the operation, yielding a pollutant-free stream for reaction or end-of-pipe methods. Conventionally, the pollutant undergoes a capture method, such as liquid scrubbing or adsorption, and is subsequently fed to a reactor system, where the VOC is incinerated or catalyzed to less harmful chemicals.[1] Recent studies have shown that concentrating the VOC-laden feed stream prior to catalytic oxidation could offer a cost-effective strategy for abatement of VOC emissions.[2] Hybrid separation and reaction has some latent advantages including minimal monetary outlay, process intensification, lower catalyst inventory, and reduced external utilities (e.g., cooling capacity and energy supply) requirements. For instance, in a two-step adsorber−incinerator process, a VOC-laden stream was concentrated over a solid adsorbent in the first bed at low temperature before it was combusted directly or catalytically in an incinerator (the second bed) for conversion to harmless compounds.[3]

Heat-integrated systems (such as honeycomb rotor adsorbers) that employ the heat of oxidation for regenerating the adsorbent were found to be a viable alternative for VOC abatement.[4,5] In such systems, one section of the bed is in adsorption mode, the next is in oxidation mode, and the following is in cooling/preheating of oxidation gas mode. Furthermore, a two-step adsorber−oxidizer system based on sintered metal fiber supported adsorbent−catalyst was investigated for the removal of a low concentration of VOCs from the air.[6] Via numerical modeling and simulation, Kolade et al.[2] studied the feasibility and applicability of the adsorptive reactor concept for VOCs oxidation, and their results demonstrated the potential advantage of this combined system. In a recent study by Wang et al.,[7] elimination of bulky aromatics such as toluene, *o*-xylene, and 1,3,5-trimethylbenzene (TMB) was investigated by a combined adsorption/combustion method over bifunctional Ru/HZSM-5.

To this end, there have been a variety of porous materials developed to remove VOCs from polluted air and industrial waste gases with activated carbons, zeolites, and silica gels being the most common candidates.[8−11] Other materials such as metal oxides and metal−organic frameworks (MOFs) have also been extensively investigated for this process.[12,13] Typically, the porous materials are used either as an adsorbent or as a catalyst support for active metals, such as transition

Received: May 21, 2020
Revised: July 2, 2020
Accepted: July 7, 2020
Published: July 7, 2020

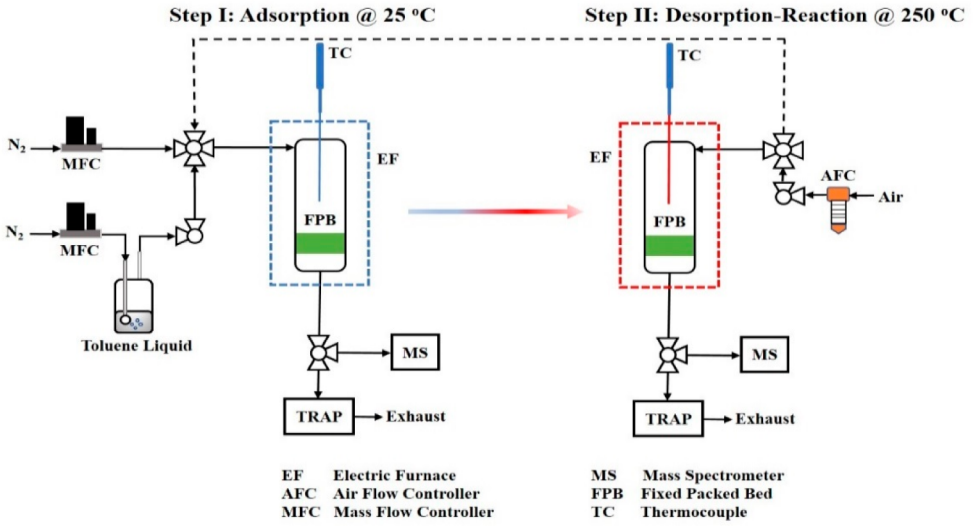

Figure 1. General scheme of the combined adsorption−reaction setup with the adsorption and desorption reaction steps.

metal cations (e.g., Cu, Co, Mn, and Fe) and noble metals (e.g., Pd, Pt, and Ru).[14−17] Carbon-based materials possess some limitations, particularly risk of ignition during thermal regeneration by hot air and reduced VOC adsorptive capacity when the relative humidity exceeds 60% mainly due to competitive adsorption. Further, the use of zeolites in the total oxidation of VOCs has certain drawbacks associated with poisoning and deactivation of the catalyst.[18] The application of metal oxide and noble metal supported catalysts in adsorption and catalytic combustion of several VOC compounds demonstrated the ability to reduce the combustion temperature significantly. In the wide range of transition metals, titania- and zirconia-based materials have been shown to have an excellent affinity toward benzene, toluene, and xylene (BTX) compounds, in particular toluene, during adsorption and reaction.[19−21] Most recently, we investigated the equilibrium and dynamic adsorption of benzene vapor over unimodal and bimodal silica-based mixed-metal oxides (MMOs) and showed the superiority of these materials in abatement of aromatic hydrocarbons.[22]

In our prior work,[23] we prepared two classes of MMOs by incorporating titania and zirconia onto a high surface area silica support with varied loadings. High porosity and large surface area along with the abundance of surface hydroxyl groups with high affinity toward carbonyl-based VOCs (i.e., formaldehyde) resulted in an efficient VOC removal performance. In this investigation, to potentially expand the utility of these materials in hybrid systems, we tested the efficacy of the aforementioned for the combined capture and destruction of toluene, as a model BTX compound. Saturated adsorption capacity was determined using pure component adsorption isotherms. Dynamic or pseudoequilibrium experiments were also performed in conjunction with the oxidation reaction to investigate the performance of the MMOs. Total oxidation was achieved using a temperature swing process to perform simultaneous adsorption and reaction, with deep oxidation being the reaction of choice due to its relatively harmless and potentially profitable byproducts.

2. EXPERIMENTAL SECTION

2.1. Materials Synthesis and Characterization. Conventional sol−gel technique was used to prepare TiO_2/SiO_2 and ZrO_2/SiO_2 MMOs. The silica chosen here was UVM-7 with a mesoporous structure, on the basis of its high surface area and ordered mesoporous structure, with hexagonal mesophases.[24] The detailed synthesis procedure along with characterization methods was provided in our previous work.[23] Briefly, zirconium(IV) propoxide or titanium(IV) butoxide with desired amounts was added to the silica synthesis solution containing tetraethyl orthosilicate (TEOS) and triethanolamine (TEAH), followed by heating to 150 °C for 1 h, then cooling to 90 °C, and addition of hexadecyltrimethylammonium bromide (CTAB). In the next step, subsequent cooling of the solution to 60 °C was carried out prior to the addition of DI water before it was set to gel at room temperature for 24 h. The final product was obtained by washing the sample with DI water and ethanol multiple times followed by drying at 80 °C overnight and subsequent calcination at 550 °C for 6 h. The TiO_2/SiO_2 samples obtained were denoted as Ti/Si-1, Ti/Si-2, Ti/Si-3, and Ti/Si-4, while the ZrO_2/SiO_2 samples were named as Zr/Si-1, Zr/Si-2, Zr/Si-3, and Zr/Si-4. The textural properties of the MMOs were evaluated by N_2 physisorption isotherms on a Micromeritics 3Flex gas analyzer at 77 K. Before these measurements, the samples were degassed at 250 °C on a Micromeritics Smart VacPrep under vacuum for 12 h. To analyze the coke formation, TGA was performed on used samples after oxidation reaction using a Q500 TA Instruments TGA, while their chemical properties were assessed by FTIR spectroscopy on a Nicolet FTIR model 750 spectrometer. To verify the chemical composition of the MMOs, XPS analysis was performed on a Kratos Axis 165 photoelectron spectrometer using an aluminum X-ray source.

2.2. Toluene Vapor Isotherm Measurements. Toluene vapor adsorption isotherms of TiO_2/SiO_2 and ZrO_2/SiO_2 samples were measured on the Micromeritics 3Flex volumetric gas analyzer at room temperature. The instrument was retrofitted with a vaporizer that carried the toluene vapor to the process chamber at saturated vapor pressure. In a typical process, toluene liquid (99%, ACS reagent grade) filled a stainless-steel vial which was attached to a heating unit that supplied the vapor to the material. For these measurements, the toluene liquid was first purified at 77 K to remove any trapped gas impurities and then vaporized at 25 °C. Around 0.1 g of the sample was then subjected to the toluene vapor for

https://dx.doi.org/10.1021/acs.iecr.0c02550
Ind. Eng. Chem. Res. XXXX, XXX, XXX−XXX

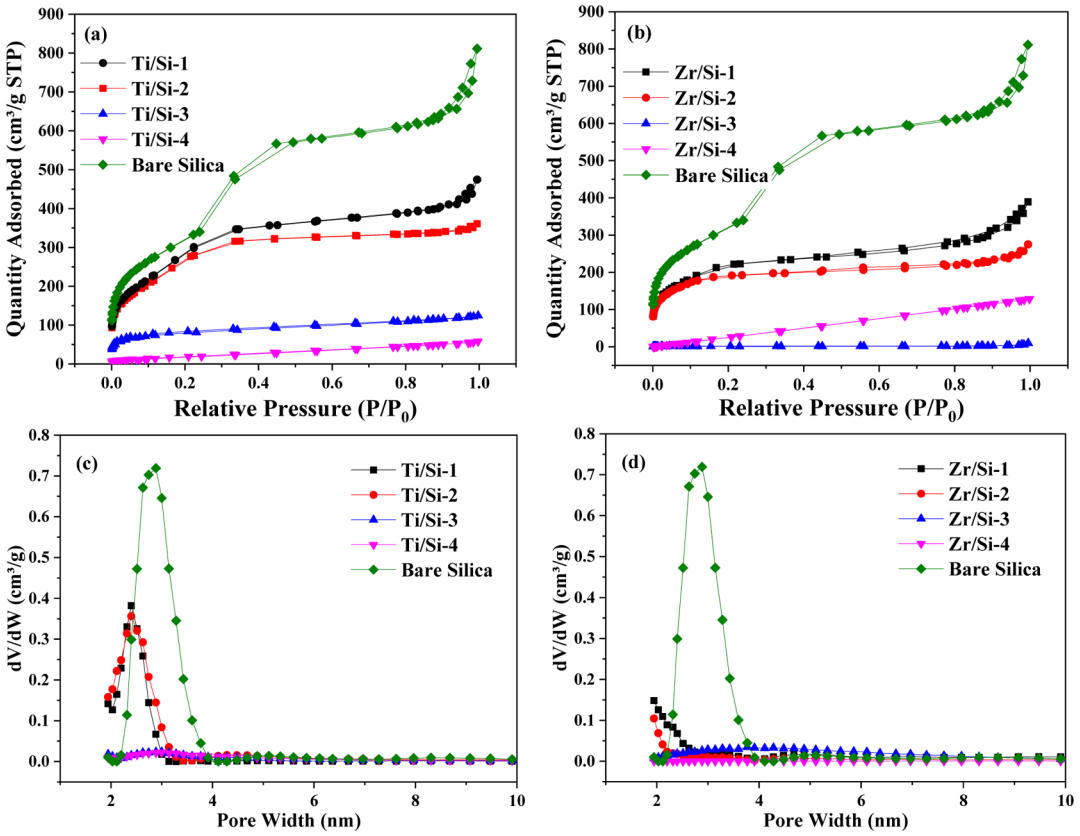

Figure 2. (a, b) N_2 physisorption isotherms and (c, d) pore size distribution profiles for (a and c) TiO_2/SiO_2 and (b and d) ZrO_2/SiO_2 samples.

an extended duration. A jacket was used to maintain the temperature in the sampling chamber at 25 °C for the duration of the experiment. Degassing of samples was done using a Micrometrics Prevac at 250 °C under vacuum for 6 h before isotherm measurements to ensure the evacuation of small molecule volatiles and condensed water molecules.

2.3. Adsorption−Reaction Experiments. Adsorption and successive oxidation were performed using a lab-scale setup illustrated in Figure 1. The bed consisted of a borosilicate glass column with a fritted silicon base to hold the bed in place. The process consisted of two steps, namely, adsorption and desorption reaction. The first step (step I) involves the delivery of toluene vapor at ~545 ppm_v carried by N_2 as a carrier gas at 60 mL/min. The sample was exposed to the inlet vapor concentration and was subjected to an adsorption process. Once the concentration of the effluent stream was detected to be of saturation levels, the carrier gas flow was halted and was followed by a temperature increase from ambient to reaction temperature (250 °C) at the beginning of step II. Previous desorption studies revealed that toluene desorbed at 75 °C. To counter the exhaustion of toluene before the reaction temperature was reached, a very low flow rate of air (21% O_2, balance N_2) was used (10 mL/min total), corresponding to a low O_2 gas hourly space velocity (GHSV) of 315 mL h^{-1} g^{-1} with respect to the weight of the bed, which has been proven to be more beneficial for toluene oxidative processes.[25] A sample weight of 0.4 g was used in the packed-bed column. Dynamic acquisition of data was achieved using an online mass spectrometer (BELMass). In sharp contrast to the adsorption process, desorption of toluene was found to be a kinetically fast process with a short time duration. The time frames for desorption varied with the percentage of metal oxide loading in the MMO materials. The interaction of preadsorbed toluene on the surface with oxygen in the introduced air facilitates the oxidative destruction of toluene, evidenced by total oxidation products (i.e., CO_2 and H_2O) produced in the majority.

3. RESULTS AND DISCUSSION

3.1. Materials Properties. The obtained N_2 physisorption isotherms are presented in Figure 2a,b. For low-loading samples (Ti/Si-1, Ti/Si-2, Zr/Si-1, and Zr/Si-2), the isotherms were found to be of combined type I−type IV isotherms, indicative of their microporous−mesoporous nature, in agreement with the UVM-7 silica support. On the other hand, for high-loading samples (Ti/Si-3, Ti/Si-4, Zr/Si-3, and Zr/Si-4), the isotherms were of type III, indicative of stronger adsorbate−adsorbate interactions. It was also noted that, at similar loadings, titania-based materials exhibited higher N_2 uptake compared to zirconia-based materials. The estimated textural properties in Table 1 showed a decreasing trend in S_{BET} and V_p with TiO_2 or ZrO_2 loading for both sets of materials. Ti/Si-1 showed a S_{BET} of 1115 m^2/g, a 25% decrease from the bare support material. Furthermore, Zr/Si-1 showed an even larger decrease of approximately 50% at 768 m^2/g. While the support material had a pore volume of 1.35 m^3/g, Ti/Si-2 showed a 53% decrease in pore volume at 0.60 m^3/g, and similar to S_{BET}, a large decrease was detected from 25 to 50 wt % loaded samples. Incorporation of 62 wt % ZrO_2 resulted in the greatest reduction in both S_{BET} and V_p for Zr/Si-4 (0.3 m^2/g and 0.01 cm^3/g, respectively) and rendered this material essentially nonporous. Moreover, it is evident from pore size distribution profiles (Figure 2c,d) that the pore size of these materials ranges from 2 to 4 nm. In addition, chemical

https://dx.doi.org/10.1021/acs.iecr.0c02550
Ind. Eng. Chem. Res. XXXX, XXX, XXX−XXX

Table 1. Textural and Chemical Properties of the MMOs and Bare Support Silica

sample	S_{BET} (m^2/g)	V_p (cm^3/g)	d_p (nm)	TiO_2 or ZrO_2 loading (wt %)
bare silica	1483	1.35	3.3	–
Ti/Si-1	1115	0.64	2.8	8
Ti/Si-2	1030	0.60	2.7	15
Ti/Si-3	271	0.18	2.7	54
Ti/Si-4	73	0.08	3.1	82
Zr/Si-1	768	0.56	2.3	13
Zr/Si-2	635	0.40	2.5	22
Zr/Si-3	226	0.18	2.5	43
Zr/Si-4	3.5	0.01	3.1	62

characterization by XPS analysis (see XPS survey spectra in Figure S1, Supporting Information) determined the TiO_2 and ZrO_2 loadings of the materials as listed in Table 1. For Ti/Si samples, the TiO_2 content ranged from 8 to 82 wt %, while for Zr/Si materials, the amount of ZrO_2 was found to be between 13 and 62 wt %. Although our initial goal was to have identical loadings for both sets of MMOs, the sol–gel synthesis method did not allow us to optimize the conditions to achieve this goal. Nevertheless, the loadings were close enough to compare their adsorption–reaction performances.

3.2. Toluene Vapor Equilibrium Adsorption Isotherms. Equilibrium adsorption capacities of the MMOs were determined by toluene vapor adsorption isotherms obtained at 25 °C across the 0–30 mmHg pressure range. The obtained isotherms are illustrated in Figure 3. In the case of Ti-based samples (Figure 3a), Ti/Si-1 exhibited the highest toluene uptake with a shape indicative of micropore filling saturation and successive multilayered adsorption and rapid mesopore capillary condensation. This material displayed an adsorption capacity of 3.9 mmol/g at 27 mmHg. Ti/Si-2 displayed a shape similar to that of its Ti/Si-1 analogue, but with a less steep initial uptake indicating internal pore diffusion controlled adsorption phenomena.[26] With the transition to higher loaded samples, a decreasing trend was obtained with a 58% drop in uptake for Ti/Si-3 at 1.4 mmol/g and a 73% drop for Ti/Si-4 at 0.9 mmol/g. Furthermore, the isotherms of Ti/Si-3 and Ti/Si-4 displayed distinctive monolayer adsorption, while the multilayer phenomenon was not observed. This could be correlated to the surface characteristics of the materials, indicating a direct correlation between textural properties and toluene uptake. In the case of ZrO_2/SiO_2 samples (Figure 3b), a similar decreasing trend was observed except for the transition from Zr/Si-3 to Zr/Si-4, which revealed an almost 2-fold increase in adsorption capacity from 0.6 to 1.2 mmol/g, despite its lower surface area and pore volume. This could be attributed to an increased number of surface hydroxyl groups, which have been hypothesized to be one of the active sites for toluene adsorption.[27] In agreement with TiO_2/SiO_2 MMOs, the stronger interaction of toluene molecules with lower loaded samples resulted in steeper isotherms at low pressures, followed by a relatively gradual increase in higher pressures. The highest toluene uptake (2.9 mmol/g) was reached over Zr/Si-1 at 27 mmHg. Comparing the toluene adsorption over these two sets of MMOs revealed that the Ti-based samples exhibited a higher affinity toward toluene, especially at lower pressures which could be the result of high dispersion of the TiO_2 particles on the SiO_2 support.[28] The Ti/Si-1 toluene isotherm, in Figure 3a, was characterized by a type II isotherm without reaching saturation, which corresponded to microporous–mesoporous adsorption processes, as mentioned earlier. This shape was expected when analyzing the interaction of nonpolar organic vapors on largely mesoporous materials.[29] On the contrary, Ti/Si-2 showed a modified type I isotherm, but the lack of a saturated point could suggest that the maximum adsorption capacity lay beyond the saturated vapor pressure of toluene; however, a rapid filling of what appears to be a monolayer phenomenon was detected by the sharp rise in the curve at approximately P = 7 mmHg. Both of the highest loaded TiO_2/SiO_2 samples (Ti/Si-3 and Ti/Si-4) illustrated a characteristic curve corresponding to type III isotherms, which are commonly associated with inefficient capture processes. This also revealed the stronger interaction of the adsorbate–adsorbate molecules when compared to the adsorbate–adsorbent interaction.[29] As shown in Figure 3b, while Zr/Si-1 showed an isotherm type similar to that of Ti/Si-1, i.e., unsaturated type II isotherm, the Zr/Si-2, Zr/Si-3, and Zr/Si-4 samples all showed a type IV isotherm with its characteristic two distinct saturation sites. This depicted the heterogeneous nature of adsorption sites on the MMO surface, providing evidence for the presence of different types of active sites. This further supported our previous findings[23] that, over these materials, both surface defects (created by the incorporation of TiO_2 or ZrO_2) and hydroxyl groups were responsible for the adsorption process.

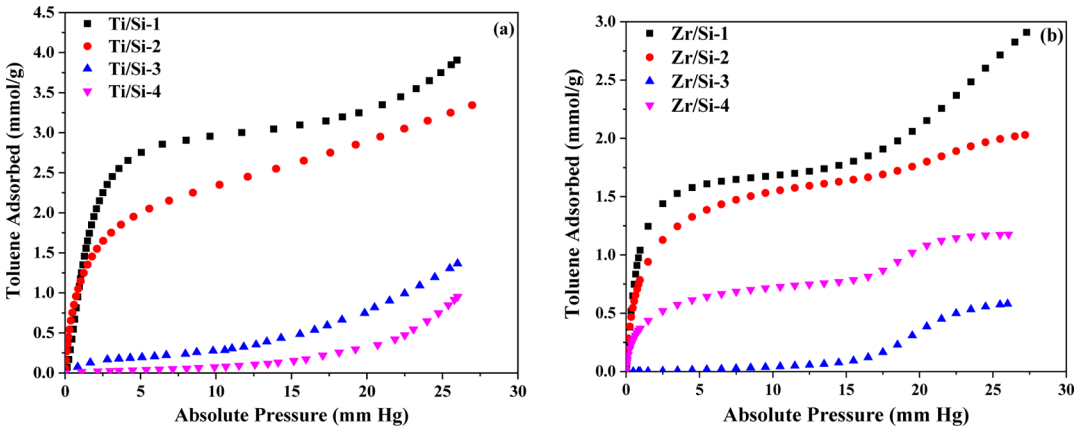

Figure 3. Toluene vapor adsorption isotherms for (a) TiO_2/SiO_2 and (b) ZrO_2/SiO_2 samples obtained at 25 °C.

https://dx.doi.org/10.1021/acs.iecr.0c02550
Ind. Eng. Chem. Res. XXXX, XXX, XXX–XXX

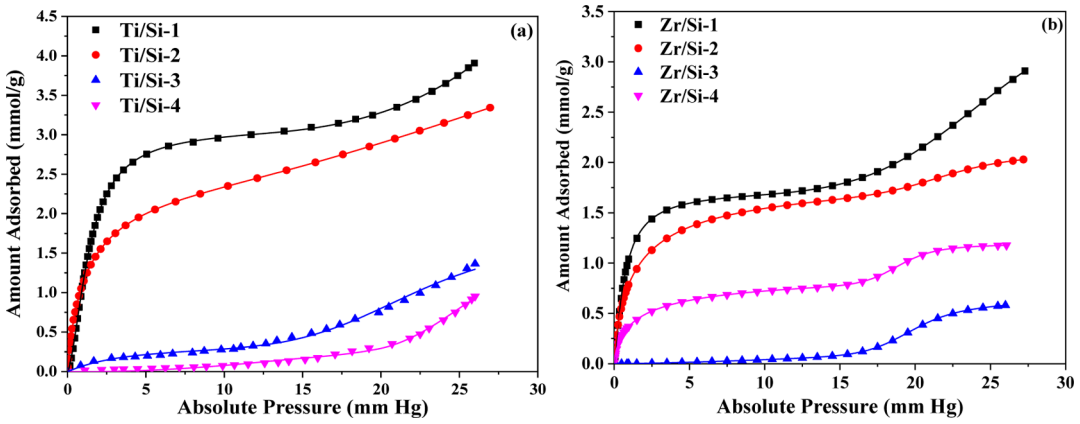

Figure 4. Isotherm fitting by DSS model for (a) TiO_2/SiO_2 and (b) ZrO_2/SiO_2 samples.

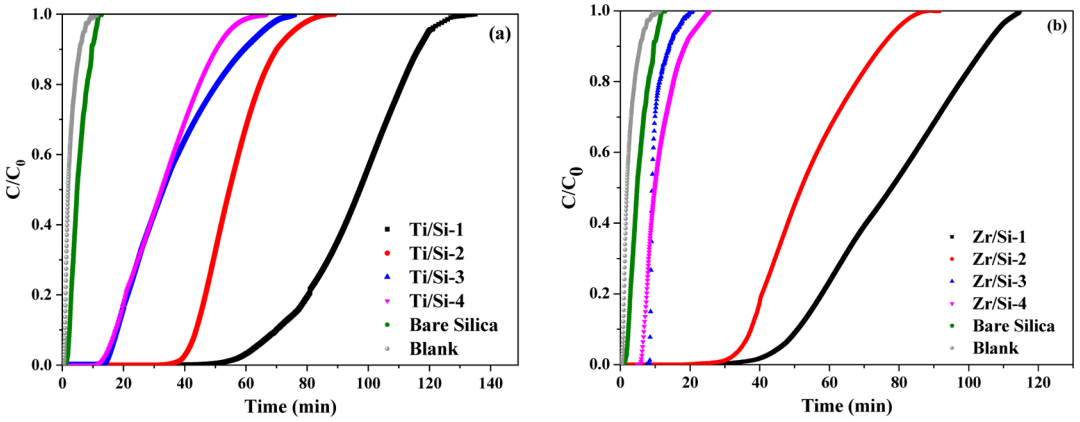

Figure 5. Toluene breakthrough profiles obtained for (a) TiO_2/SiO_2 and (b) ZrO_2/SiO_2 samples.

The level of heterogeneity was seen to be greater for ZrO_2/SiO_2 samples, as illustrated by the different saturation levels.

Nonlinear curve fitting was used to determine adsorption parameters.[30] We used various adsorption isotherm models including single-site Langmuir, Toth, dual-site Langmuir (DSL), and dual-site Sips (DSS) to describe the experimental trends. The equations and their corresponding parameters are provided in the Supporting Information. Among these models, the DSS model was found to give the best fit with the lowest regression with R^2 values greater than 0.99, as displayed in Table S1, Supporting Information. The fitted isotherms with the DSS model are illustrated in Figure 4. While most of the TiO_2/SiO_2 samples showed a smaller deviation in the Toth model when compared to the Langmuir model, Ti/Si-4 showed the highest R^2 for the latter, which suggested primarily the monolayer adsorption phenomenon in this case. This was further evidenced by the far lower regression obtained in the Langmuir model when compared to other models, as seen in Table S1. Furthermore, the larger R^2 values for the DSS model further enforced the hypothesis of the existence of multiple adsorption sites. Detailed statistics about the DSS model can be found in Table S2, Supporting Information.

3.3. Dynamic Adsorption Performance. Breakthrough experiments were performed to assess the dynamic adsorption performance of the prepared materials for the abatement of toluene. The dynamic (pseudoequilibrium) adsorption capacity, q_d, of the MMOs was calculated by using eq 1:

$$q_d = \frac{Q_0 C_0 t_s}{m} \tag{1}$$

where Q_0 (mL/min) is the volumetric flow rate of the feed entering the bed, C_0 (mmol/mL) corresponds to the feed concentration, m (g) is the mass of adsorbent loaded onto the packed-bed column, and t_s (min) is the total or stoichiometric time, which can be calculated from eq 2:

$$t_s = \int_0^\infty \left(1 - \frac{C}{C_0}\right) dt \tag{2}$$

where C is the toluene concentration at the reactor outlet at time t.

Figure 5 shows toluene breakthrough profiles over the studied MMOs. Blank profiles were included with the others to show the hydrodynamics of the empty column, while silica profiles were included as a control. As expected, bare silica showed the shortest breakthrough and saturation times among the adsorbents, implying its lower toluene capacity than those of MMOs. While the surface (interior and exterior) of bare silica terminates in O−H groups, which subsequently function as its only active sites, the MMOs had a combination of O−H groups and the surface defects created by functionalizing with secondary metal oxides which gave rise to higher toluene affinity. Among the two groups of the MMO samples, Ti-based materials (Figure 5a) depicted longer breakthrough and saturation times and hence exhibited a much higher dynamic adsorption capacity when compared to Zr-based materials (Figure 5b) in agreement with their higher equilibrium

https://dx.doi.org/10.1021/acs.iecr.0c02550
Ind. Eng. Chem. Res. XXXX, XXX, XXX−XXX

behavior, as noted earlier. Moreover, it can be seen in Figure 5 that, within each group of the MMOs, the breakthrough time decreased with loading. However, in agreement with what was observed in isotherm measurements, Zr/Si-3 and Zr/Si-4 samples depicted intersecting profiles thereby giving Zr/Si-4 higher saturation time than the Zr/Si-3 counterpart, though Zr/Si-3 still maintained a longer breakthrough than Zr/Si-4.

An important parameter in breakthrough profile analysis is the concentration front steepness. Other than between Zr/Si-3 and Zr/Si-4, the steepness of the breakthrough profiles increased fairly with loading, thereby leading to faster adsorption kinetics, as quantitatively depicted by the values of the breakthrough width (Table 2). For the Ti-based samples, toluene breakthrough width increased from 8.9 min for bare silica to 56.8, 27.4, 48.1, and 39.0 min, while the Zr-based counterparts gave rise to breakthrough widths of 63.0, 44.6, 7.9, and 15.6 min as loading increased. From these results, it was evident that the adsorption of toluene was heavily diffusion-controlled, and was enhanced by the presence of hydroxyl groups,[31] which could explain the 62% increase in capacity from Zr/Si-3 to Zr/Si-4. While the adsorption capacities of the lower loaded samples were higher, the extended long tail of the breakthrough curve represented a slow and limiting process.

Table 2. Dynamic Adsorption Data for MMO Materials Obtained from Breakthrough Profiles

sample	$t_{5\%}$ (min)	$t_{50\%}$ (min)	$t_{95\%}$ (min)	breakthrough width (min)	q_d (mmol/g)
blank	0.7	1.9	7.2	6.5	–
bare silica	2.0	4.9	10.9	8.9	0.1
Ti/Si-1	63.0	92.7	119.7	56.8	3.8
Ti/Si-2	41.6	54.7	69.3	27.4	3.3
Ti/Si-3	16.0	32.7	66.0	49.1	1.3
Ti/Si-4	15.5	32.5	54.8	39.0	0.9
Zr/Si-1	46.0	78.0	109.0	63.0	2.9
Zr/Si-2	34.9	52.0	79.5	44.6	2.0
Zr/Si-3	8.5	10.0	16.4	7.9	0.5
Zr/Si-4	6.3	9.9	21.9	15.6	1.2

The values of some of the important adsorption parameters calculated from the breakthrough profiles are shown in Table 2. In particular, Ti/Si-1 showed the highest dynamic adsorption capacity of 3.8 mmol/g at C/C_0 = 0.95, which was close to its equilibrium capacity shown in Figure 4a, while Ti/Si-2 exhibited a capacity of 3.3 mmol/g. Higher doped Ti-based materials displayed a remarkable drop in toluene uptake as Ti/Si-4 showed ca. 76% reduction in toluene capacity relative to Ti/Si-1. Similarly, among the Zr-based samples, Zr/Si-1 the highest dynamic adsorption capacity at 2.9 mmol/g, while Zr/Si-about 30% drop in capacity at C/C_0 = 0.95. However, Zr/Si-4 showed adsorption capacity of 1.2 mmol/g, more than twice the value for Zr/Si-3 hypothesized to be due to its higher number of surface OH groups. This was indicative of the surface properties and their role in toluene adsorption, as the highest loaded samples demonstrated a small amount of accessible surface area. The lowest loaded samples of each class depicted superior dynamic capacities relative to the higher loaded samples, with a decrease in efficiency with progressively higher loadings. Bare silica, despite having superior surface characteristics, showed a very small capacity at 0.1 mmol/g. This indicated that the doping of the metal oxide resulted in properties significant to toluene capture, which could be attributed to surface hydroxyl groups and active sites

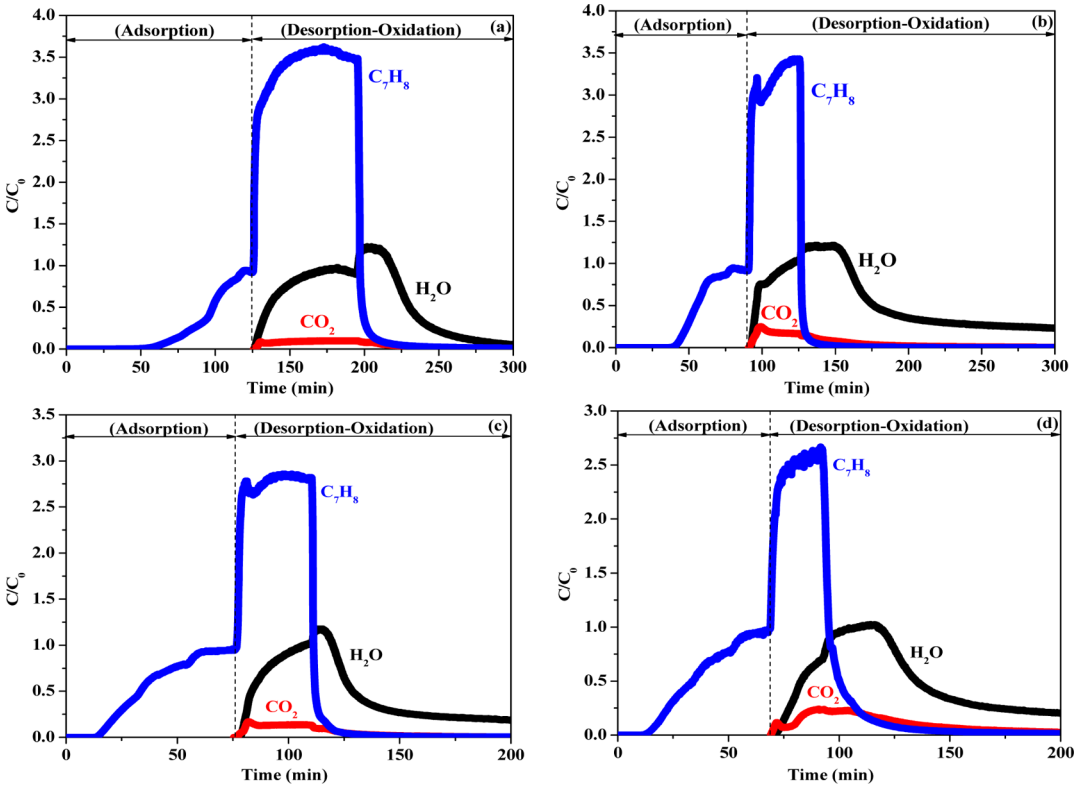

Figure 6. Adsorption−reaction profiles for TiO_2/SiO_2 samples: (a) Ti/Si-1, (b) Ti/Si-2, (c) Ti/Si-3, and (d) Ti/Si-4.

https://dx.doi.org/10.1021/acs.iecr.0c02550
Ind. Eng. Chem. Res. XXXX, XXX, XXX−XXX

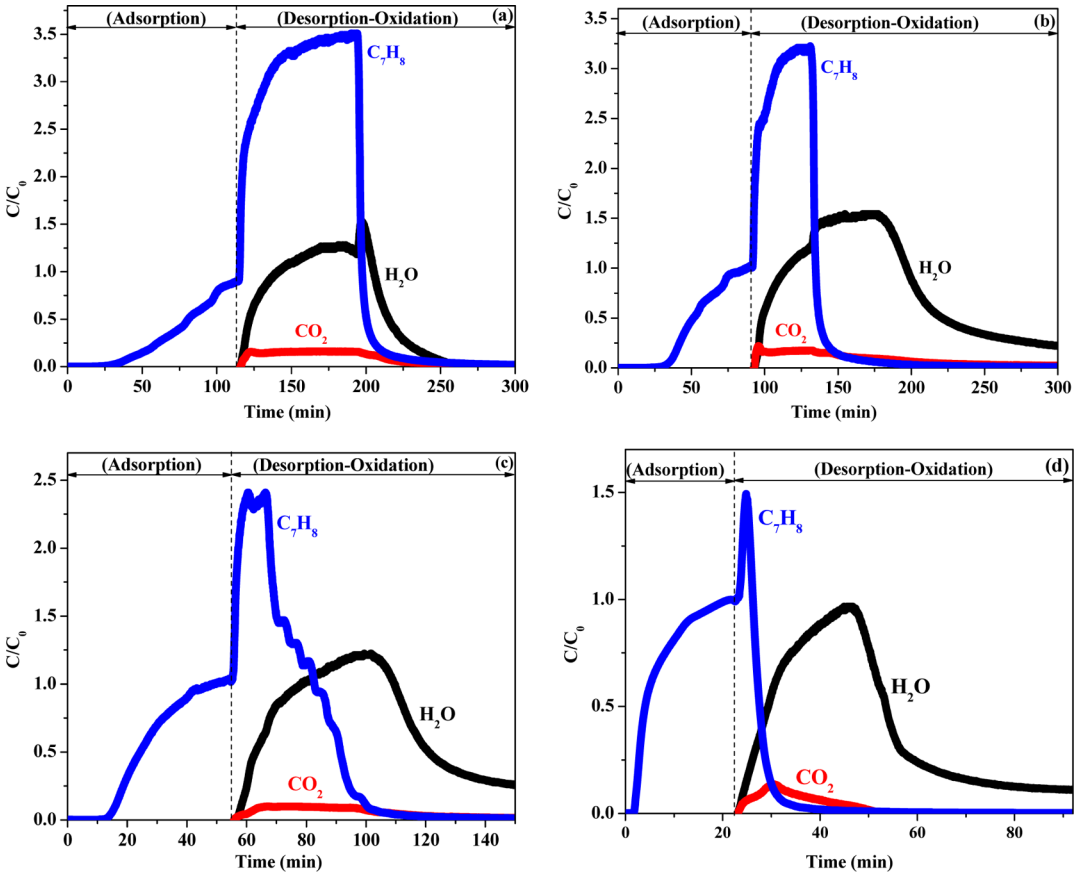

Figure 7. Adsorption−reaction profiles for ZrO_2/SiO_2 samples: (a) Zr/Si-1, (b) Zr/Si-2, (c) Zr/Si-3, and (d) Zr/Si-4.

introduced by the incorporation of Ti or Zr. In all, Ti/Si-1 showed the highest adsorption capacity at 3.8 mmol/g, around 2% less than the equilibrium measurements performed earlier.

3.4. Combined Adsorption−Reaction Performance. Following adsorption at room temperature, regenerative airflow was introduced to the bed at 10 mL/min to maintain a low O_2 GHSV, while the temperature was ramped to 250 °C at a rate of 10 °C/min. It is worth mentioning ab initio that only C_7H_8, CO_2, and H_2O profiles are shown in the reaction plots (Figures 6 and 7) because N_2 and O_2 were well in excess amounts throughout the reaction. The desorption of toluene was detected at around 75 °C, while product formation was observed shortly after. Figure 6 illustrates the breakthrough/oxidation profiles obtained for Ti-based MMOs. First, the transition from adsorption to desorption−oxidation started with initial roll-ups from C/C_0 = 1 to 3.7, 3.4, 2.8, and 2.6 for 70, 37, 35, and 25 min for Ti/Si-1, Ti/Si-2, Ti/Si-3, and Ti/Si-4, respectively, in agreement with the dynamic adsorption capacities of the samples. These initial roll-ups above the toluene adsorption step inlet concentration, C_0, were due to the net positive concentration of the gas-phase (inter- and intraparticle) toluene inside the bed after adsorption saturation, the amount desorbed, and the amount reacted. Hence, during this period, the rate of oxidation of gas-phase toluene was less than its rate of desorption plus the amount of its remnant at the end of adsorption. Immediately after this stage, toluene concentration started decreasing as shown in Figure 6 since the remnant of gas-phase toluene at the end of adsorption had been completely pushed out of the bed or otherwise reacted while the rate of desorption was greater than the rate of oxidation. Therefore, the excess of desorption over oxidation could be inferred as the amount of toluene detected. Moreover, Ti/Si-1 and Ti/Si-2 exhibited a noticeable high rate of formation of total oxidation products (Figure 6a,b) when compared to the higher loaded Ti/Si-3 and Ti/Si-4 (Figure 6c,d), indicated by the delayed time frames under the curve. Considering the areas under the graphs, we could infer that the amounts of CO_2 and H_2O produced decreased with loading.

As for Figure 7 for the Zr-based materials, it is needless to describe the entire profiles because as shown they followed trends similar to those observed in Figure 6 for Ti-based materials. However, Zr-based materials exhibited slower reaction kinetics relative to the Zr-based analogues. This was easily noticeable from the toluene profile slope during the oxidation step. It was also noticeable that, while the amount of CO_2 produced decreased, the amount of H_2O produced increased with loading.

From both Figures 6 and 7, we noted that the concentration of H_2O was much higher than that of CO_2 against the established reaction stoichiometry, which could be correlated to possible high-temperature adsorption of the produced CO_2 by the adsorbents. Another noticeable trend in Figures 6 and 7 was that the rate of desorption decreased with metal loading, as revealed by the decreasing slopes of the desorption profiles. This may be attributed to pore blockage created by the higher loading thereby causing a barrier for fast diffusion in the adsorbent pores.[28] Likewise, coke formation for both classes of materials was discovered to be minimal and will be further revealed by the TGA results. This had been found in the past to be a crucial factor in aromatic oxidative reactions.[32] Notably,

https://dx.doi.org/10.1021/acs.iecr.0c02550
Ind. Eng. Chem. Res. XXXX, XXX, XXX−XXX

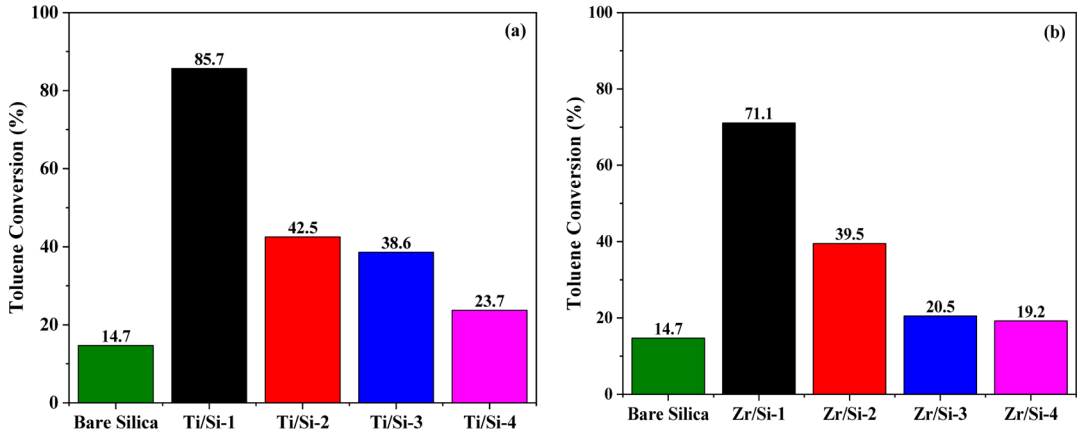

Figure 8. Toluene overall conversion for bare SiO_2 and (a) TiO_2/SiO_2 samples and (b) ZrO_2/SiO_2 samples for catalytic oxidation carried out at 250 °C.

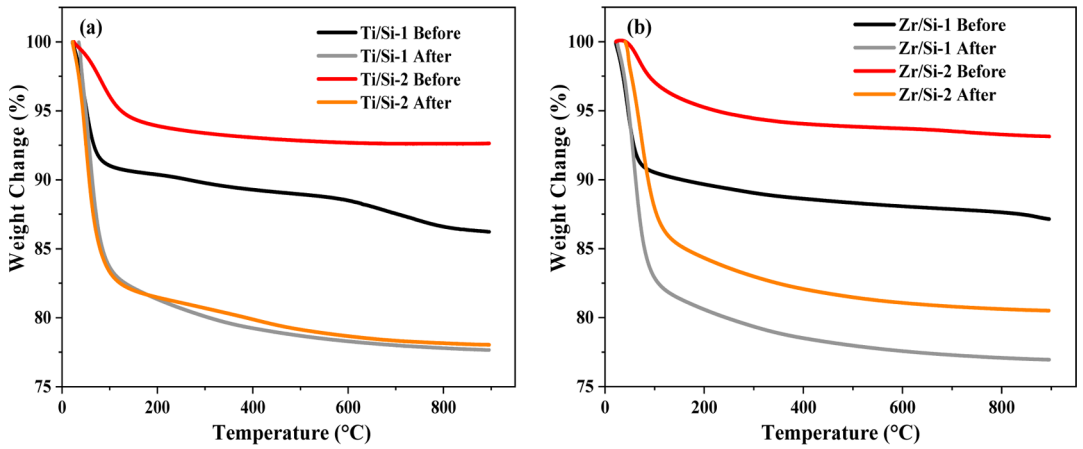

Figure 9. TGA analysis for (a) Ti/Si-1 and Ti/Si-2 samples and (b) Zr/Si-1 and Zr/Si-2 samples before and after oxidation.

minor quantities of benzaldehyde, a partial oxidation product, were detected as well; however, the mole fraction was quantified to be a differential amount and was therefore not represented here.

Figure 8 represents the toluene overall conversion over both series of adsorbents. The data was evaluated against expected stoichiometric values and was measured from the toluene desorption at about 75 °C. As revealed in Figure 8a, Ti/Si-1 showed the highest conversion of toluene (86%) when compared to other materials. Similar to the adsorption characteristics, a decrease in conversion was observed from Ti/Si-1, to Ti/Si-2, to Ti/Si-3, and to Ti/Si-4 which could be due to limited surface area for catalytic oxidation of toluene. Moreover, the presence of high loading on the SiO_2 support could act as a resistance to diffusion of reactant oxygen to the catalytic active sites thereby leading to a decrease in conversion as loading increases. Shown in Figure 8b is the toluene conversion for the ZrO_2/SiO_2 samples and the bare silica. As expected and similar to the Ti/Si-1 sample, Zr/Si-1 depicted a maximum conversion of about 71% relative to the bare silica and other zirconia samples. This high conversion could be related to its higher surface area and pore volume, which not only enhanced the adsorption rate but also provided more active sites for subsequent reaction.[33] Linking with Figures 6 and 7, it should be noted that the area under toluene C/C_0 concentration after the end of roll-up perfectly correlated with the conversion. The low conversion of high-loading samples could be linked to their limited surface area and most likely to a low degree of ZrO_2 or TiO_2 particle dispersion on the SiO_2 surface, as a result of particle agglomeration, which not only reduced their dynamic capacity but also catalytic activity. It should be noted that catalytic oxidations of VOCs on MMOs are affected by many factors as the loading of doped metal is changed; namely, particle dispersion, changing kinetics, and accessibility of active sites are all contributors to these observed trends. As proposed here, concentrating toluene prior to its oxidation improved the catalytic performance mainly because, according to previously published data in the literature,[34,35] the majority of titania- and zirconia-based catalytic oxidations without prior feed concentration (i.e., adsorption step) typically exhibited low conversions at reaction temperatures of ~250 °C. Nevertheless, deconvolution of many effects of prior feed concentration on the catalytic performance of the materials are needed for further optimization of these materials. Such analyses which are the focus of continuing work will allow for determination of the critical aspects of MMOs-based adsorptive reactors. Rostami et al.[36] conducted adsorptive thermocatalytic oxidation of BTX using a clinoptilolite (a natural zeolite) adsorbent bed and combined Fe^0 and Cu_2O nanoparticle catalyst bed, and they recorded a maximum conversion of 96% at 400 °C. However, upon decreasing the temperature to 300 °C, only 85% conversion was achieved. A few other researchers have used different dual-functional materials and recorded conversions

https://dx.doi.org/10.1021/acs.iecr.0c02550
Ind. Eng. Chem. Res. XXXX, XXX, XXX−XXX

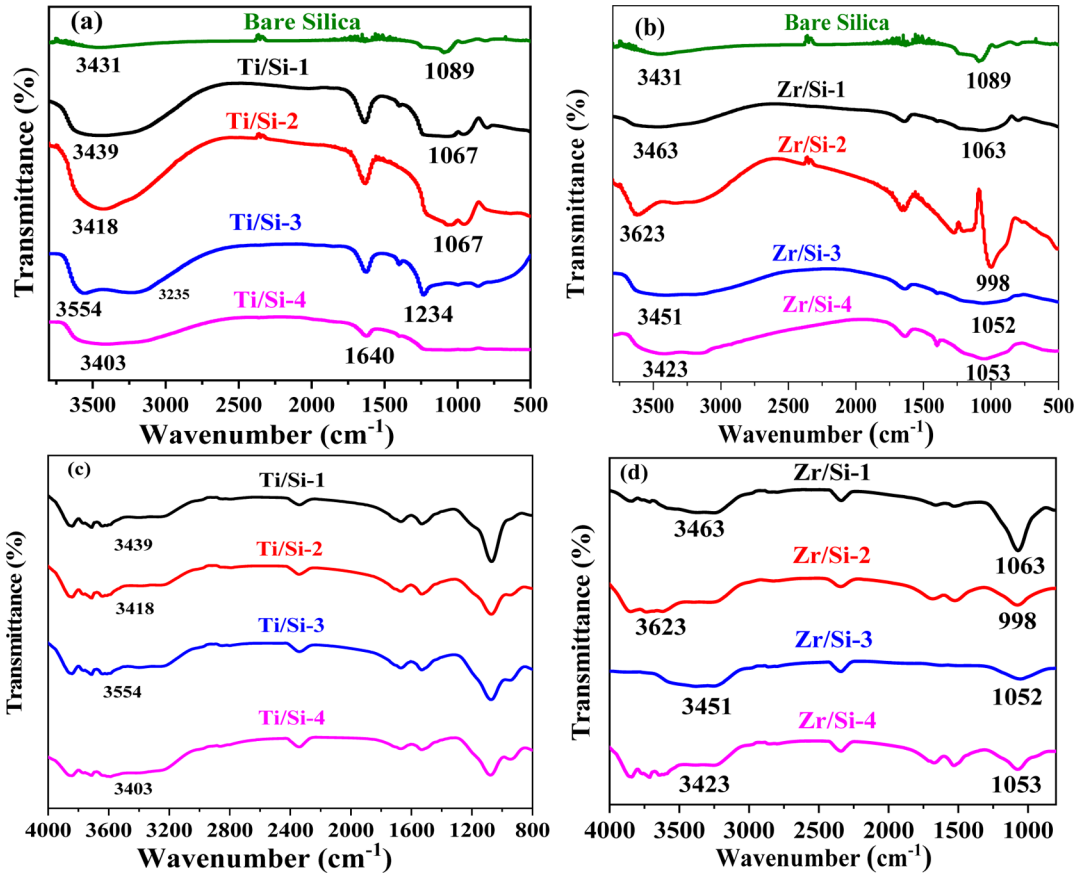

Figure 10. FTIR spectra for fresh (a) TiO_2/SiO_2 and (b) ZrO_2/SiO_2 samples and spent (c) TiO_2/SiO_2 and (d) ZrO_2/SiO_2 samples after catalytic oxidation at 250 °C.

close to the values recorded here, though at different conditions.[1,37] On the basis of catalytic performance and materials cost, it is conclusive that the dual-functional materials tested in this study can compete favorably with the few dual-functional materials that have been investigated so far for VOC abatement.

To ascertain the level of coking over the MMOs during the oxidation reaction, lower-loading fresh (before) and spent (after) materials (Ti/Si-1&2 and Zr/Si-1&2) were evaluated for weight loss by TGA in the temperature range 25−900 °C. The results are provided in Figure 9. While the 15% fresh samples showed about 13% loss, the 25% samples displayed a 7% loss. These weight losses could be due to the remnant of the surfactant used in the synthesis of the materials or the removal of preadsorbed water on the surface. Relative to the fresh samples, it was clear that spent samples had a minimal level of coke formation (maximum of 15%) during the oxidation reaction. As shown in Figure 9a, Ti/Si-1 displayed a maximum coke formation of about 10%, whereas Ti/Si-2 displayed about 15%. A similar trend was also observed between the higher-loading zirconia samples (Figure 9b): Zr/Si-1 exhibited 12% and Zr/Si-2 14% maximum coke formation. On the basis of these results, it was evident that toluene oxidation over silica-based MMOs gave rise to a low degree of coke formation.

To chemically characterize the materials after the oxidation process, FTIR spectroscopic analysis was performed on all the MMOs before and after the reaction, the results of which are shown in Figure 10. Present in all the materials was a band detected in the range 1000−1250 cm^{-1}. This band could be attributed to a basic functional group of these materials. In addition, SiO_4 and Si−O−Si absorption bands were observed in this range, indicating the role of silica as a support cum building block for the MMOs. An absorption band was detected close to 950 cm^{-1}, which was linked to the presence of the Si−O−Ti/Zr stretching vibration. Moreover, the presence of O−H groups in the materials was confirmed by the broad peaks detected beyond 3000 cm^{-1}, the broadness of which was due to O−H stretching vibrations. For the fresh Ti-based materials, Figure 10a, serial low-intensity peaks were also detected in the range 500−700 cm^{-1}, indicating the presence of anatase-phase titania within the TiO_2/SiO_2 MMOs.[38] Furthermore, as loading increased, the vibrational modes of SiO_4 shifted, thereby suggesting structural defects within the silica support. Surface H−O−H, under bending modes, was attributed to the peaks detected around 1639 cm^{-1} as a result of chemisorbed water on the surface of the materials,[39] while surface O−H was responsible for the peaks in the range 3235−3554 cm^{-1}. Quantitatively, the largest concentration of surface O−H groups was found in Ti/Si-1, in agreement with what was observed earlier in the pseudoequilibrium adsorption measurements. Moreover, a sequential decrease in O−H concentration was observed as titania loading increased. Shown in Figure 10b are FTIR spectra of the Zr-based materials. Neumayer et al.[40] assigned the peaks in 998−1063 cm^{-1} to asymmetric stretching of the SiO_4 group. Another peak was found around 1050−1063 cm^{-1}, which could be attributed to the presence of SiO_4^- tetrahedra.

https://dx.doi.org/10.1021/acs.iecr.0c02550
Ind. Eng. Chem. Res. XXXX, XXX, XXX−XXX

After the oxidation process (Figure 10c,d), the O−H groups intensity reduced in concentration, an indication that these functional groups were responsible for some of the active sites. This would explain the reason for better capacity and conversion at lower loadings. A peak at 2300 cm^{-1} was detected after the oxidation process in both classes of materials, which could correspond to unreacted toluene or partial oxidation products still bonded to the catalyst. By comparing the FTIR spectra of the fresh (Figure 10a,b) and the spent (Figure 10c,d) materials, it was conclusive that adsorption and/or reaction affected the structure of both classes of MMO materials.

4. CONCLUSIONS

This paper gives insight into a hybrid adsorption−reaction process that utilizes MMOs for the abatement of toluene, as a model BTX compound. The adsorption potential of toluene on the MMOs was determined by isotherm and breakthrough measurements. Across materials investigated, Ti/Si-1 and Zr/Si-1 were found to exhibit the highest toluene vapor uptake under both equilibrium and dynamic conditions. Ti/Si-1, among the Ti-based samples, displayed highest dynamic adsorption capacity at 3.8 mmol/g at 1 bar and 25 °C with toluene feed concentration of ∼550 ppm_v. Similarly, among the Zr-based samples, Zr/Si-1 displayed the highest capacity at 2.9 mmol/g under the same conditions. Except between Zr/Si-3 and Zr/SI-4, both classes of materials showed a downward trend in capacity with an increase in loading percentages. The maximum toluene adsorption capacity of 3.9 mmol/g was achieved over Ti/Si-1 at 27 mmHg and 25 °C. Nonlinear curve fitting analysis revealed the existence of multiple adsorption sites for toluene on the MMOs. Moreover, the dynamic adsorption−reaction tests revealed the superior nature of low-loaded MMOs relative to their high-loaded counterparts. This was in agreement with the equilibrium adsorption measurements, which revealed a direct correlation between separation efficiency and conversion. Ti/Si-1 and Zr/Si-1 showed toluene conversions of 86 and 71%, respectively. Due to conventionally low temperatures for the oxidation process, low quantities of partial oxidation products were also obtained, such as benzaldehyde. Post oxidative chemical analysis confirmed the existence of hydroxyl groups as active sites for toluene adsorption and oxidation. However, no major changes in the chemical structure were detected, along with no observable coke formation on the surface of the catalyst after the process, which reveals the potential of these materials to function as dual-functional materials with potentially high reusability.

■ ASSOCIATED CONTENT

Supporting Information

The Supporting Information is available free of charge at https://pubs.acs.org/doi/10.1021/acs.iecr.0c02550.

Additional XPS spectra of TiO_2/SiO_2 and ZrO_2/SiO_2 samples, equilibrium adsorption fitting using Langmuir, Toth, and dual-site Sips (DSS) isotherm models, regression analysis of the different isotherm models, and DSS parameters (PDF)

■ AUTHOR INFORMATION

Corresponding Author

Fateme Rezaei − *Department of Chemical & Biochemical Engineering, Missouri University of Science and Technology, Rolla, Missouri 65409, United States;* orcid.org/0000-0002-4214-4235; Email: rezaeif@mst.edu

Authors

Busuyi O. Adebayo − *Department of Chemical & Biochemical Engineering, Missouri University of Science and Technology, Rolla, Missouri 65409, United States*

Anirudh Krishnamurthy − *Department of Chemical & Biochemical Engineering, Missouri University of Science and Technology, Rolla, Missouri 65409, United States*

Ali A. Rownaghi − *Department of Chemical & Biochemical Engineering, Missouri University of Science and Technology, Rolla, Missouri 65409, United States;* orcid.org/0000-0001-5228-5624

Complete contact information is available at: https://pubs.acs.org/10.1021/acs.iecr.0c02550

Notes

The authors declare no competing financial interest.

■ ACKNOWLEDGMENTS

The authors thank the National Science Foundation (NSF CBET-1802049) for financially supporting this project.

■ REFERENCES

(1) Esparza-Isunza, T.; López-Isunza, F. Modeling the Transient VOC (Toluene) Oxidation in a Packed-Bed Catalytic Reactor. *Int. J. Chem. React. Eng.* **2016**, *14* (6), 1177−1185.

(2) Kolade, M. A.; Kogelbauer, A.; Alpay, E. Adsorptive Reactor Technology for VOC Abatement. *Chem. Eng. Sci.* **2009**, *64* (6), 1167−1177.

(3) Kullavanijaya, E.; Trimm, D. L.; Cant, N. W. Adsocat: Adsorption/Catalytic Combustion for VOC and Odour Control. *Stud. Surf. Sci. Catal.* **2000**, *130*, 569−574.

(4) Campesi, A.; Luzi, C. D.; Martínez, O. M.; Barreto, G. Effect of Concentration by Thermal Swing Adsorption on the Catalytic Incineration of VOCs. *Int. J. Chem. React. Eng.* **2012**, *10* (A54), 1−22.

(5) Yamauchi, H.; Kodama, A.; Hirose, T.; Okano, H.; Yamada, K. I. Performance of VOC Abatement by Thermal Swing Honeycomb Rotor Adsorbers. *Ind. Eng. Chem. Res.* **2007**, *46* (12), 4316−4322.

(6) Nikolajsen, K.; Kiwi-Minsker, L.; Renken, A. Structured Fixed-Bed Adsorber Based on Zeolite/Sintered Metal Fibre for Low Concentration VOC Removal. *Chem. Eng. Res. Des.* **2006**, *84* (7), 562−568.

(7) Wang, Y.; Yang, D.; Li, S.; Chen, M.; Guo, L.; Zhou, J. Ru/Hierarchical HZSM-5 Zeolite as Efficient Bi-Functional Adsorbent/Catalyst for Bulky Aromatic VOCs Elimination. *Microporous Mesoporous Mater.* **2018**, *258*, 17−25.

(8) Heinen, A. W.; Peters, J. a.; van Bekkum, H. Competitive Adsorption of Water and Toluene on Modified Activated Carbon Supports. *Appl. Catal., A* **2000**, *194*−*195*, 193−202.

(9) Huang, Q.; Vinh-Thang, H.; Malekian, A.; Eić, M.; Trong-On, D.; Kaliaguine, S. Adsorption of N-Heptane, Toluene and o-Xylene on Mesoporous UL-ZSM5Materials. *Microporous Mesoporous Mater.* **2006**, *87* (3), 224−234.

(10) Rokicińska, A.; Drozdek, M.; Dudek, B.; Gil, B.; Michorczyk, P.; Brouri, D.; Dzwigaj, S.; Kuśtrowski, P. Cobalt-Containing BEA Zeolite for Catalytic Combustion of Toluene. *Appl. Catal., B* **2017**, *212*, 59−67.

(11) Zhang, J.; Rao, C.; Peng, H.; Peng, C.; Zhang, L.; Xu, X.; Liu, W.; Wang, Z.; Zhang, N.; Wang, X. Enhanced Toluene Combustion Performance over Pt Loaded Hierarchical Porous MOR Zeolite. *Chem. Eng. J.* **2018**, *334*, 10−18.

(12) Song, L.; Zhang, J.; Sun, L.; Xu, F.; Li, F.; Zhang, H.; Si, X.; Jiao, C.; Li, Z.; Liu, S.; et al. Mesoporous Metal−Organic

Frameworks: Design and Applications. *Energy Environ. Sci.* **2012**, *5* (6), 7508−7520.
(13) Galli, S.; Masciocchi, N.; Colombo, V.; Maspero, A.; Palmisano, G.; López-Garzón, F. J.; Domingo-Garcia, M.; Fernández-Morales, I.; Barea, E.; Navarro, J. a R. Adsorption of Harmful Organic Vapors by Flexible Hydrophobic Bis-Pyrazolate Based MOFs. *Chem. Mater.* **2010**, *22* (5), 1664−1672.
(14) Rooke, J. C.; Barakat, T.; Siffert, S.; Su, B.-L. Total Catalytic Oxidation of Toluene Using Pd Impregnated on Hierarchically Porous Nb_2O_5 and Ta_2O_5 Supports. *Catal. Today* **2012**, *192* (1), 183−188.
(15) Hosseini, M.; Barakat, T.; Cousin, R.; Aboukaïs, A.; Su, B. L.; De Weireld, G.; Siffert, S. Catalytic Performance of Core-Shell and Alloy Pd-Au Nanoparticles for Total Oxidation of VOC: The Effect of Metal Deposition. *Appl. Catal., B* **2012**, *111−112*, 218−224.
(16) Barakat, T.; Rooke, J. C.; Tidahy, H. L.; Hosseini, M.; Cousin, R.; Lamonier, J. F.; Giraudon, J. M.; De Weireld, G.; Su, B. L.; Siffert, S. Noble-Metal-Based Catalysts Supported on Zeolites and Macro-Mesoporous Metal Oxide Supports for the Total Oxidation of Volatile Organic Compounds. *ChemSusChem* **2011**, *4* (10), 1420−1430.
(17) Krishnamurthy, A.; Adebayo, B.; Gelles, T.; Rownaghi, A.; Rezaei, F. Abatement of Gaseous Volatile Organic Compounds: A Process Perspective. *Catal. Today* **2020**, *350*, 100−119.
(18) Gelles, T.; Krishnamurthy, A.; Adebayo, B.; Rownaghi, A.; Rezaei, F. Abatement of Gaseous Volatile Organic Compounds: A Material Perspective. *Catal. Today* **2020**, *350*, 3−18.
(19) Zou, L.; Luo, Y.; Hooper, M.; Hu, E. Removal of VOCs by Photocatalysis Process Using Adsorption Enhanced TiO_2-SiO_2 Catalyst. *Chem. Eng. Process.* **2006**, *45* (11), 959−964.
(20) Li, W. B.; Wang, J. X.; Gong, H. Catalytic Combustion of VOCs on Non-Noble Metal Catalysts. *Catal. Today* **2009**, *148* (1−2), 81−87.
(21) Blount, M. C.; Falconer, J. L. Steady-State Surface Species during Toluene Photocatalysis. *Appl. Catal., B* **2002**, *39* (1), 39−50.
(22) Adebayo, B. O.; Lawson, S.; Rownaghi, A. A.; Rezaei, F. Analysis of Equilibrium and Dynamic Adsorption of Benzene Vapor over Unimodal and Bimodal Silica-Based Mixed-Metal Oxides. *Chem. Eng. J.* **2020**, *396*, 125273.
(23) Krishnamurthy, A.; Thakkar, H.; Rownaghi, A. A.; Rezaei, F. Adsorptive Removal of Formaldehyde from Air Using Mixed-Metal Oxides. *Ind. Eng. Chem. Res.* **2018**, *57* (38), 12916−12925.
(24) Fenelonov, V. B.; Romannikov, V. N.; Derevyankin, A. Y. Mesopore Size and Surface Area Calculations for Hexagonal Mesophases (Types MCM-41, FSM-16, Etc.) Using Low-Angle XRD and Adsorption Data. *Microporous Mesoporous Mater.* **1999**, *28* (1), 57−72.
(25) Viinikainen, T. S.; Lehtonen, J. S. Toluene Oxidation in the Absence and Presence of CO, CO_2, Water and H_2 over ZrO_2-Based Gasification Gas Clean-Up Catalysts. *ChemistrySelect* **2017**, *2* (4), 1663−1670.
(26) Lee, J. S.; Adams, R. T.; Madden, W.; Koros, W. J. Toluene and N-Heptane Sorption in Matrimid® Asymmetric Hollow Fiber Membranes. *Polymer* **2009**, *50* (25), 6049−6056.
(27) Ncube, T.; Kumar Reddy, K. S.; Al Shoaibi, A.; Srinivasakannan, C. Benzene, Toluene, m-Xylene Adsorption on Silica-Based Adsorbents. *Energy Fuels* **2017**, *31* (2), 1882−1888.
(28) Ortiz De Zárate, D.; Gómez-Moratalla, A.; Guillem, C.; Beltrán, A.; Latorre, J.; Beltrán, D.; Amorós, P. High-Zirconium-Content Nano-Sized Bimodal Mesoporous Silicas. *Eur. J. Inorg. Chem.* **2006**, *2006* (13), 2572−2581.
(29) Keller, J. U.; Staudt, R. *Gas Adsorption Equilibria: Experimental Methods and Adsorptive Isotherms*; Springer: Boston, 2005.
(30) Ayawei, N.; Ebelegi, A. N.; Wankasi, D. Modelling and Interpretation of Adsorption Isotherms. *J. Chem.* **2017**, *2017*, 1−11.
(31) Seo, H. O.; Kim, D. H.; Kim, K. D.; Park, E. J.; Sim, C. W.; Kim, Y. D. Adsorption and Desorption of Toluene on Nanoporous TiO_2/SiO_2 Prepared by Atomic Layer Deposition (ALD): Influence of TiO_2 Thin Film Thickness and Humidity. *Adsorption* **2013**, *19* (6), 1181−1187.
(32) Miyata, H.; Mukai, T.; Ono, T.; Ohno, T.; Hatayama, F. Fourier-Transform Infrared Investigation of Intermediates in the Oxidation of Toluene on V_2O_5/TiO_2. *J. Chem. Soc., Faraday Trans. 1* **1988**, *84* (7), 2465−2475.
(33) Przekop, R. E.; Kirszensztejn, P. Highly Dispersed Pt on B_2O_3/Al_2O_3 Support: Catalytic Properties in the Total Oxidation of 1-Butene. *React. Kinet., Mech. Catal.* **2016**, *118* (1), 325−335.
(34) Viinikainen, T.; Kouva, S.; Lehtonen, J.; Kanervo, J. Toluene Oxidation over ZrO_2-Based Gasification Gas Clean-up Catalysts: Part A. Effect of Oxygen and Temperature on the Product Distribution. *Appl. Catal., B* **2016**, *199*, 523−530.
(35) Viinikainen, T.; Kouva, S.; Lehtonen, J.; Kanervo, J. Toluene Oxidation over ZrO_2-Based Gasification Gas Clean-up Catalysts: Part B. *Appl. Catal., B* **2016**, *199*, 45−54.
(36) Rostami, R.; Jonidi Jafari, A. Application of an Adsorptive-Thermocatalytic Process for BTX Removal from Polluted Air Flow. *J. Environ. Health Sci. Eng.* **2014**, *12* (89), 1−9.
(37) Campesi, M.; Luzi, C.; Barreto, F.; Martinez, M. Evaluation of an Adsorption System to Concentrate VOC in Air Streams Prior to Catalytic Incineration. *J. Environ. Manage.* **2015**, *154*, 216−224.
(38) Adamczyk, A.; Długoń, E. The FTIR Studies of Gels and Thin Films of Al_2O_3-TiO_2 and Al_2O_3-TiO_2-SiO_2 Systems. *Spectrochim. Acta, Part A* **2012**, *89*, 11−17.
(39) Yu, J.; Zhao, X.; Yu, J.; Zhong, G.; Han, J.; Zhao, Q. The Grain Size and Surface Hydroxyl Content of Super-Hydrophilic TiO_2/SiO_2 Composite Nanomeer Thin Films. *J. Mater. Sci. Lett.* **2001**, *20*, 1745−1748.
(40) Neumayer, D. A.; Cartier, E. Materials Characterization of ZrO_2−SiO_2 and HfO_2−SiO_2 Binary Oxides Deposited by Chemical Solution Deposition. *J. Appl. Phys.* **2001**, *90* (4), 1801−1808.

https://dx.doi.org/10.1021/acs.iecr.0c02550
Ind. Eng. Chem. Res. XXXX, XXX, XXX−XXX